Coexistence of type-II Dirac point and weak topological phase in Pt_{3}Sn

Minsung Kim, Cai-Zhuang Wang, and Kai-Ming Ho

Phys. Rev. B **96**, 205107 — Published 6 November 2017

DOI: 10.1103/PhysRevB.96.205107

Coexistence of type-II Dirac point and weak topological phase in Pt_3Sn

Minsung Kim, Cai-Zhuang Wang, and Kai-Ming Ho
Ames Laboratory, US DOE and Department of Physics and Astronomy, Iowa State University, Ames, Iowa 50011, USA
(Dated: October 19, 2017)

Intriguing topological phases may appear in both insulating and semimetallic states. Topological insulators exhibit topologically nontrivial band inversion, while topological Dirac/Weyl semimetals show "relativistic" linear band crossings. Here, we report an unusual topological state of Pt_3Sn, where the two topological features appear simultaneously. Based on first-principles calculations, we show that Pt_3Sn is a 3D weak topological semimetal with topologically nontrivial band inversion between the valence and conduction bands, where the band structure also possesses type-II Dirac points at the boundary of two electron pockets. The formation of the Dirac points can be understood in terms of the representations of relevant symmetry groups and the compatibility relations. The topological surface states appear in accordance with the nontrivial bulk band topology. The unique coexistence of the two distinct topological features in Pt_3Sn enlarges the material scope in topological physics, and is potentially useful for spintronics.

I. INTRODUCTION

Topological physics has been one of the most intriguing findings in condensed matter physics[1–4]. The topological aspect of electronic structures was first noted in quantum Hall effects[5,6], and further extended to systems where the topological nature is protected under time-reversal symmetry ($\mathbb{Z}_2$ topological insulators[7–12]) or point-group symmetry (topological crystalline insulators[13–15]). In these systems, the topologically nontrivial character remains robust as long as the gap is kept finite. Recently, another important classes of the topological material in metallic systems, i.e., Dirac/Weyl semimetals[3,16–23] were also discovered. In Dirac semimetals, the band crossing between two (spin-degenerate) bands occurs, forming a linear Dirac cone which is reminiscent of a relativistic massless particle. The Dirac points in topological Dirac materials can appear on high-symmetry paths of the Brillouin zone (BZ), and are protected by relevant group symmetry[17,18,21].

Although the two topological phases in gapped and gapless systems were discovered and defined separately, in principle an electronic band structure may possess the two topological features simultaneously. The topological character of a topological insulator can be extended to a semimetallic band structure since the topological classification is valid as long as the direct gap at each k-point of the BZ is kept finite. In this case, the band structure has electron and hole pockets while the nontrivial band inversion remains robust. This enables the possibility to have an additional topological character in the same system because a topological band crossing (e.g., Dirac point) in the electron or hole pockets may appear near the Fermi level. However, a specific material example with the coexisting topological features has not been reported yet.

In this study, we show that Pt_3Sn has such an unusual band structure with the dual topological nature. We perform first-principles calculations based on density functional theory to show that Pt_3Sn is a weak topological semimetal characterized by nontrivial weak $\mathbb{Z}_2$ invariants. The semimetallic band structure exhibits electron and hole pockets, and accidental band crossings in the conduction bands give rise to Dirac points near the Fermi energy. While the conventional Dirac points occur at the boundary between the valence and conduction bands, the Dirac points in Pt_3Sn appear within the conduction bands in which the dispersion of the low-lying conduction bands leads to type-II Dirac points[24] that violate the Lorentz invariance, and thus are not allowed in high-energy physics (Fig. 1). Representative Dirac points appear near the Fermi level at the boundary of two electron pockets. The Dirac points are protected by relevant point group symmetry, and their formation is explained by the group representations and the compatibility relations. Topological surface states are confirmed to be consistent with the bulk topological character. We also discuss the topologically nontrivial band splitting between the two conduction bands constituting the Dirac points under anisotropic strain.

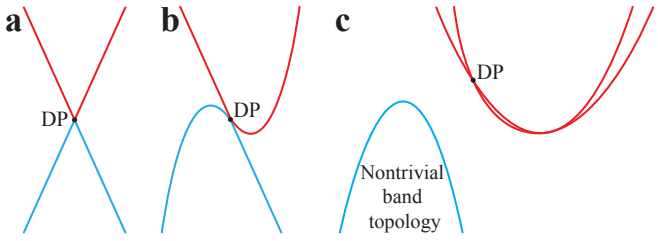

FIG. 1. Schematic illustrations of different Dirac points and band topology. (a) Conventional Dirac point (DP). (b) Type-II Dirac point at the boundary of electron and hole pockets. (c) In Pt_3Sn, type-II Dirac points appear at the boundary of two electron pockets and the valence band has nontrivial band topology (detailed analysis for the valence band topology will be presented below by calculating the parities of the wavefunctions).

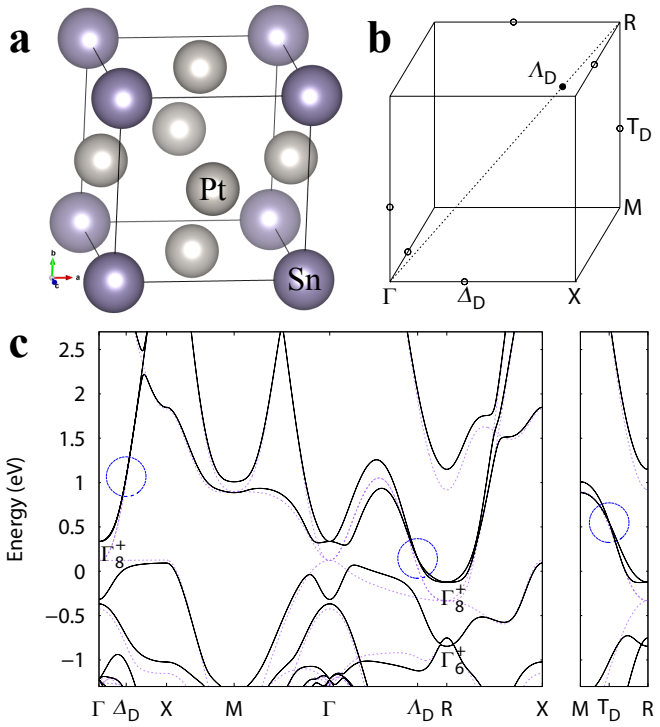

FIG. 2. Atomic and electronic structure of Pt_3Sn. (a) Atomic structure of Pt_3Sn and (b) the corresponding BZ. (c) Electronic band structure along high-symmetry paths in the BZ. The solid (dotted) lines denote the calculations with SOC (without SOC). The Fermi level is set to 0.

II. THEORETICAL METHODS

The electronic structure was calculated using density functional theory as implemented in VASP package[25,26]. PAW (projector augmented wave) method[27] was used, and the energy cutoff for the plane-wave basis was set to 383 eV. We employed PBE (Perdew-Burke-Ernzerhof) exchange-correlation functional[28] and $15 \times 15 \times 15$ k-point sampling. The effect of the spin-orbit coupling (SOC) was included. Experimental lattice constant was used[29]. For the surface state calculation, 41-layer slab in (001) direction with a sufficient vacuum region (≈ 25Å) was adopted. The electronic structure was also checked and the symmetry representation was analyzed using WIEN2k package[30].

III. RESULTS AND DISCUSSIONS

The crystal structure of Pt_3Sn has cubic symmetry with the space group $Pm\bar{3}m$ (No. 221) as illustrated in Fig. 2a. Experimentally, Pt_3Sn has been studied regarding the electronic structure[31], the atomic structure[29], the surface structure[32–36], the oxygen adsorption[37,38], the catalytic properties[39], etc. However, the topological features of the electronic structure have not been noticed. The electronic band structure has semimetallic character (Fig. 2c) where hole pockets appear along Γ–X in the BZ that compensate electron pockets around R in agreement with previous theoretical and experimental studies[31,40]. Here, due to the simultaneous presence of the spatial inversion and the time-reversal symmetry, all bands are spin-degenerate (in our DFT and DFT+U calculations we find that Pt_3Sn does not have a ferromagnetic ground state in accordance with experiments). The bands near the Fermi energy is mostly derived from Pt $5d$ states. We note that when the spin-orbit coupling is not included, the band structure shows gapless feature. However, upon including the spin-orbit coupling, the degeneracy at Γ and R is lifted to have direct gaps, which results in the semimetallic band structure. The conduction band minimum lies at the R point of the BZ, and the symmetry representation of the lowest conduction bands at R is Γ_8^+ of the (double) group O_h, which came from Γ_4^+ by the spin-orbit splitting via $\Gamma_4^+ \otimes \Gamma_6^+ = \Gamma_6^+ \oplus \Gamma_8^+$ (Fig. 2c), where the size of the spin-orbit splitting is calculated to be ≈ 0.72 eV. Similarly, the low-lying conduction bands at Γ has the Γ_8^+ representation.

The band crossings in the two (spin-degenerate) lowest conduction bands occur at several points in the BZ (marked by the dashed-line circles in Fig. 2c), which constitute the type-II Dirac points. In particular, the energy E_{Λ_D} of the Dirac points at Λ_D in Γ–R direction lie near the Fermi level E_F with $E_{\Lambda_D} - E_F \approx 0.14$ eV. The Dirac points at Λ_D are protected by the point group symmetry C_{3v}. In general, two bands with different symmetry can cross without hybridization since hybridization is forbidden when they belong to different representations. Thus, a Dirac point can be developed when such a band crossing occurs on a high-symmetry line in the BZ[17,18,41]. Along Γ–R direction, the two conduction bands belong to the representations Γ_4 and $\Gamma_5 + \Gamma_6$, respectively (Fig. 3a), as dictated by the compatibility relation $O_h : \Gamma_8^+ \rightarrow C_{3v} : \Gamma_4 + \Gamma_5 + \Gamma_6$. The two different representations show different behavior under the symmetry operations; for example, they have different eigenvalues with respect to the 3-fold rotation, i.e., $e^{\pm i\pi/3}$ for Γ_4 and -1 for $\Gamma_5 + \Gamma_6$. The type-II Dirac points occur at the boundary of two electron pockets (Fig. 3b, c, d, e), which is a distinctive feature of Pt_3Sn.

Similarly, the band crossings also occur along R–M and Γ–X to give rises to Dirac points. The relevant point group symmetry in these cases is C_{4v}, where the low-lying conduction bands constituting the Dirac points belong to two different representations Γ_6 and Γ_7 (since the compatibility relation is $O_h : \Gamma_8^+ \rightarrow C_{4v} : \Gamma_6 + \Gamma_7$). In contrast, along R–X the symmetry is not sufficiently high to give rise to a Dirac band crossing. Here, the relevant point group symmetry is C_{2v}. Since the low-lying conduction bands belong to the same representation Γ_5 ($O_h : \Gamma_8^+ \rightarrow C_{2v} : 2\Gamma_5$), which is the only two-dimensional representation of C_{2v}, they do not cross, but develop a small hybridization gap. Note that whether a band crossing along a high symmetry path is allowed can be directly read off from the compatibility relation.

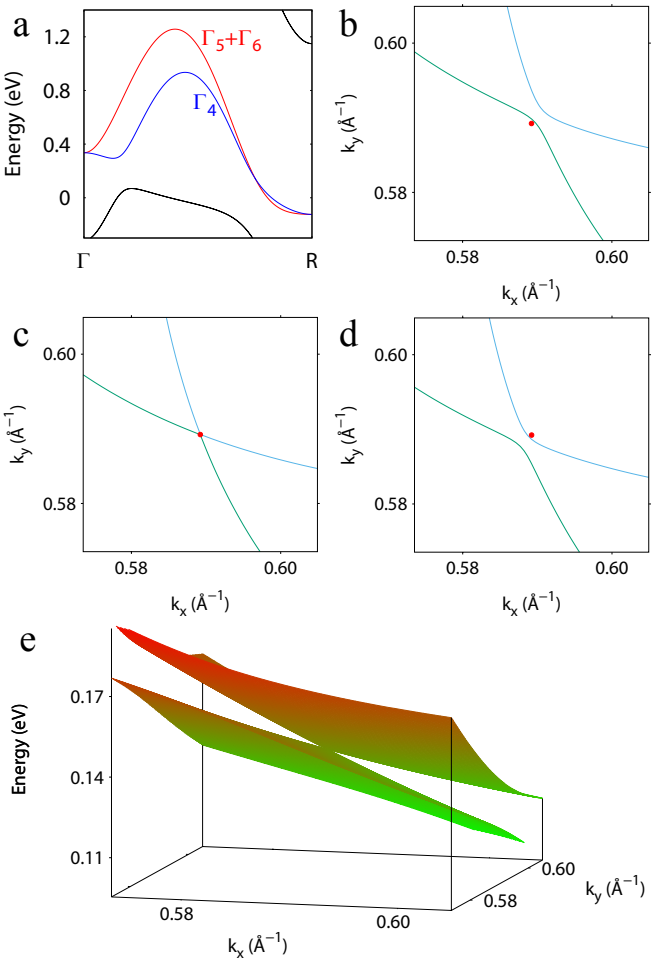

FIG. 3. Electronic band structure near the Dirac point along Γ–R. (a) The band structure and representations of the low-lying conduction bands along Γ–R. The constant energy lines ($E = E_{\Lambda_D}$) are depicted near the Dirac point in k_x–k_y planes with (b) $k_z = \frac{1}{\sqrt{3}}k_D - 0.001 \times \frac{2\pi}{a}$ (c) $k_z = \frac{1}{\sqrt{3}}k_D$ (d) $k_z = \frac{1}{\sqrt{3}}k_D + 0.001 \times \frac{2\pi}{a}$ where the Dirac point is located at $\frac{1}{\sqrt{3}}(k_D, k_D, k_D)$ with the energy E_{Λ_D}. The red circles denote (projected) positions of the Dirac point. (e) The band dispersion in the vicinity of the Dirac point.

The effective Hamiltonian for the type-II Dirac points can be constructed by considering the invariant terms under the relevant symmetry[42]. For the Dirac points at Λ_D along Γ–R, the symmetry to be considered is C_{3v} and the combination of the spatial inversion $\mathcal{I}$ and the time-reversal $\mathcal{T}$. The basis functions of the Γ_4 and $\Gamma_5 + \Gamma_6$ representations can be represented by $\left|j = \frac{1}{2}, m = \pm\frac{1}{2}\right\rangle$ and $\left|j = \frac{3}{2}, m = \pm\frac{3}{2}\right\rangle$, respectively. By considering the transformation rules under the symmetry operations of C_{3v} and $\mathcal{IT}$, the effective Hamiltonian near the Dirac point at Λ_D can be written as

$$\begin{aligned}\mathcal{H}_{\Lambda_D} &= \epsilon_{\Lambda_D} + v_t k_z + v_3 k_z \sigma_3 \otimes \mathbb{I}_{2\times2} \\ &\quad + v_1 \{k_x \sigma_1 \otimes \mathbb{I}_{2\times2} - k_y \sigma_2 \otimes \sigma_3\} \\ &\quad + v_2 \{k_x \sigma_2 \otimes \sigma_2 + k_y \sigma_2 \otimes \sigma_1\} \end{aligned} \quad (1)$$

$$= \epsilon_{\Lambda_D} + \begin{pmatrix} (v_t+v_3)k_z & 0 & v_1 k_+ & -v_2 k_+ \\ 0 & (v_t+v_3)k_z & v_2 k_- & v_1 k_- \\ v_1 k_- & v_2 k_+ & (v_t-v_3)k_z & 0 \\ -v_2 k_- & v_1 k_+ & 0 & (v_t-v_3)k_z \end{pmatrix}, \quad (2)$$

where σ_i are Pauli matrices, $\mathbb{I}_{2\times2}$ is the 2×2 identity matrix, $k_+ = k_x + ik_y$, $k_- = k_x - ik_y$, the local k_z axis at the Dirac point is set along the (111) direction, and $\hbar$ is suppressed for notational simplicity. The corresponding eigenvalues are given by

$$E_\pm = \epsilon_{\Lambda_D} + v_t k_z \pm \sqrt{v_\perp^2 (k_x^2 + k_y^2) + v_3^2 k_z^2}, \quad (3)$$

where ϵ_{Λ_D} is the energy of the Dirac point, v_t describes the "tilting" of the Dirac cone, and $v_\perp^2 \equiv v_1^2 + v_2^2$. Note that each eigenvalue appears twice due to the spin degeneracy from the $\mathcal{I}$ and $\mathcal{T}$ symmetry. From the first-principles calculations, we find that $|v_t| \approx 5.3 \times 10^4$m/s, $|v_3| \approx 5.6 \times 10^3$m/s, and $|v_\perp| \approx 1.9 \times 10^4$m/s. In particular, since $|v_t| > |v_3|$ and $|v_\perp| \neq |v_3|$, we have an anisotropic type-II Dirac cone at Λ_D. The effective Hamiltonian at the Dirac point Λ_D may look mathematically analogous to that of silicene[43,44] since the symmetry group D_3 of silicene at the K point of the BZ is isomorphic to C_{3v}. However, there are important differences that should be noted; i) the Dirac cones of silicene are gapped by intrinsic SOC whereas the Dirac cones in Pt_3Sn are not. When SOC is considered, silicene is known to be a 2D topological insulator[45]. ii) the Dirac points of silicene are 2D type-I as opposed to the 3D type-II Dirac points in Pt_3Sn.

Now we discuss the band topology of the valence bands in Pt_3Sn. Due to the time-reversal symmetry and direct gap at each k point, the band topology of the valence bands can be defined and characterized by conventional $\mathbb{Z}_2$ topological invariants[10]. Since the inversion symmetry is present, the $\mathbb{Z}_2$ topological invariants can be calculated by the parity products of the wavefunctions at time-reversal invariant momenta[46]. According to our first-principles calculations, the topological indices are $(\nu_0; \nu_1\nu_2\nu_3) = (0; 111)$, where ν_0 is the strong topological index and ν_1, ν_2, ν_3 are weak ones (Fig. 4a). Thus, Pt_3Sn has a weak topological phase in (111) direction which can be interpreted as stacked layers of 2D topological phases[10].

The topological surface states appear in accordance with the bulk topological invariants (Fig. 4). The projected parity products in the surface BZ dictate the number (mod 2) of crossings of the surface bands with a line connecting two time-reversal invariant momenta in the bulk direct gap. For instance, along $\overline{\Gamma}$–$\overline{X}$, $\overline{\Gamma}$ and $\overline{X}$ have different parities, hence we have odd number of crossings (i.e., a single crossing) of the surface states (Fig. 4b, c). In contrast, along $\overline{\Gamma}$–$\overline{M}$, we have the same parities, resulting in even number of crossings. This confirms the

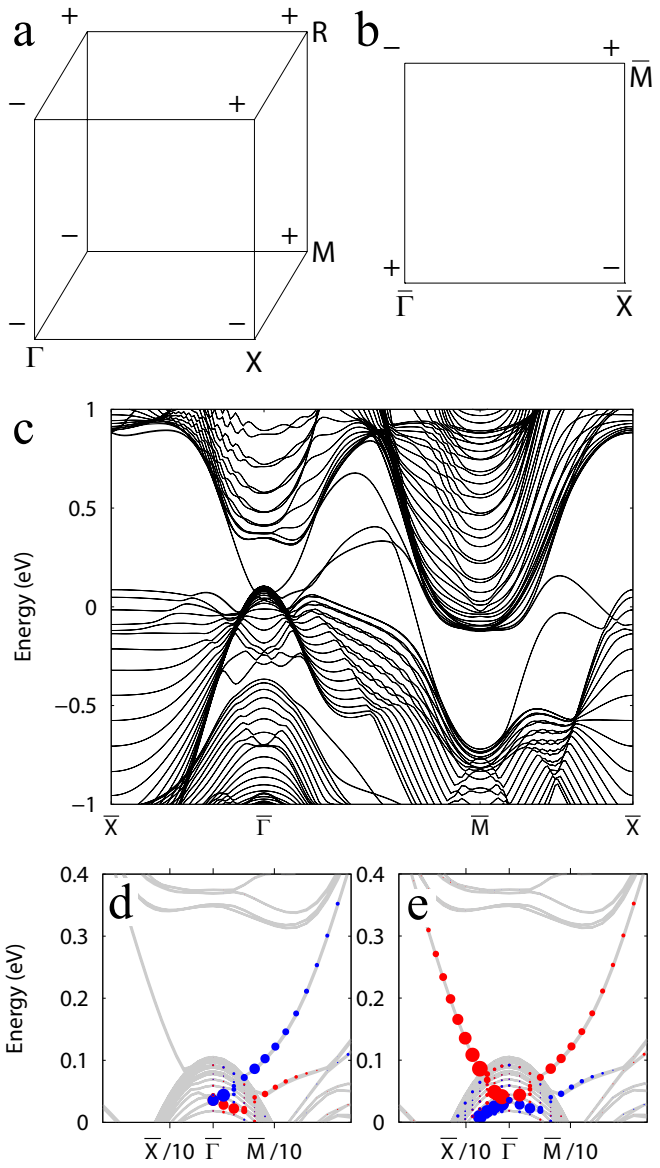

FIG. 4. Topological surface states of Pt_3Sn. (a) The parity products at the time-reversal invariant momenta in the bulk BZ and (b) the projected values in the surface BZ are presented. (c) The electronic band structure of the (001) surface. The (d) x and (e) y components of the spin projection of surface states near $\overline{\Gamma}$, where the red and blue colors mean the positive and negative values, respectively. Here, $\overline{X}/10 = (\pi/10a, 0)$ and $\overline{M}/10 = (\pi/10a, \pi/10a)$.

bulk-boundary correspondence between the bulk topological numbers and the surface state configurations. Also, the spin projection of the topological surface states is presented in Fig. 4d and e, in which they show typical helical spin texture.

The topological band splitting between the low-lying conduction bands constituting the Dirac points can be investigated by applying anisotropic strain to the system. A Dirac material can be a neighboring phase to other topological phases[17,18,21], and perturbation can make the

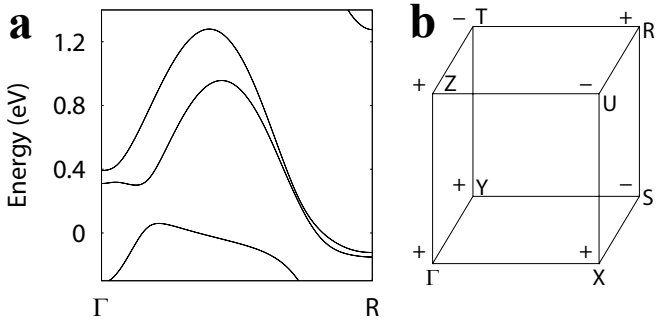

FIG. 5. Topological band splitting of the low-lying conduction bands under the anisotropic strain. (a) Band dispersion along Γ–R. (c) Parities at the time-reversal invariant momenta.

Dirac cone massive by breaking the related symmetry to induce a topological phase transition. Here, we consider anisotropic strain in which we apply 0%, 1%, 2% of compressive strain along x, y, z directions, respectively (i.e., the lattice constants are changed to be a, 0.99a, 0.98a in x, y, z directions, respectively, where the three lattice vectors remain orthogonal) while the internal (fractional) coordinates of the constituent atoms are kept fixed. This separates the two lowest conduction bands at all k points; the anisotropic strain beaks the 3-fold and 4-fold symmetry of the system and opens small gaps in the Dirac cones, and the degeneracy at Γ and R is also lifted due to the lowered symmetry (Fig. 5a). Then the band topology of the lowest conduction band can be defined. Since the inversion symmetry is preserved under the anisotropic strain, the topological invariants can be still calculated from the parities, which is $(\nu_0; \nu_1\nu_2\nu_3) = (1; 000)$ according to our calculation (Fig. 5b). Thus, the anisotropic strain opens gaps at Dirac points to induce the topologically nontrivial band splitting between the two low-lying conduction bands. (Note that the topological indices (1;000) are those of the lowest conduction band under the anisotropic strain, and the topological indices of the valence band are still (0;111) since the direct gap at each k-point between the valence and conduction bands remains finite under the anisotropic strain.)

In general, a Dirac point is composed of Weyl points with opposite chirality[17]. If the inversion symmetry or the time-reversal symmetry is broken, a Dirac point will split into Weyl points. In our system, breaking of the time-reversal symmetry via magnetic doping could be feasible experimentally, which would induce type-II Weyl points.

Experimentally, the topological electronic structure could be checked by angle resolved photoemission spectroscopy (ARPES). Since the Dirac point lies above the Fermi level, electron doping would be needed to access the Dirac point using ARPES. According to our density of states calculation, doping of 0.12 electrons per formula unit is needed for the shift of the Fermi level by 0.14 eV assuming rigid band shift, which could be feasible in experiments. We note that the energy separation

of the Dirac bands along Gamma to X is relatively small, which would make it difficult to confirm experimentally. Also, in view of surface transport, a bulk-insulating phase could be more desirable than a bulk-semimetallic phase. While Pt_3Sn has a weak topological phase, a strong topological phase would be advantageous in that they have robust topological surface states regardless of the surface direction. In these regards, further investigation in the Pt-Sn family would be interesting for future studies.

IV. CONCLUSION

In summary, we presented and theoretically analyzed a hitherto unnoticed topological electronic structure of Pt_3Sn which has unusual coexistence of the two distinct topological characters. The lowest conduction bands develop type-II Dirac points along high symmetry paths in the BZ, and the valence bands have nontrivial band topology. The group representations and the compatibility relations explain the formation of Dirac points. The valence bands are in a weak topological phase, and the configuration of the topological surface state is consistent with the bulk band topology. Recently, Dirac node arcs in an another intermetallic compound $PtSn_4$ have been studied using ARPES[47]. Our results show a distinctive example of a topological material which could be useful for future spintronic applications.

ACKNOWLEDGMENTS

This work was performed at Ames laboratory which is operated for the U.S. Department of Energy by Iowa State University under Contract No. DE-AC02-07CH11358, and supported by the U.S. Department of Energy, Office of Basic Energy Sciences, Division of Materials Sciences and Engineering. Computations were performed through the support of the National Energy Research Scientific Computing Center (NERSC) which is a DOE Office of Science User Facility supported by the Office of Science of the U.S. Department of Energy under Contract No. DE-AC02-05CH11231.

[1] M. Z. Hasan and C. L. Kane, Rev. Mod. Phys. **82**, 3045 (2010).
[2] X.-L. Qi and S.-C. Zhang, Rev. Mod. Phys. **83**, 1057 (2011).
[3] A. Bansil, H. Lin, and T. Das, Rev. Mod. Phys. **88**, 021004 (2016).
[4] C.-K. Chiu, J. C. Y. Teo, A. P. Schnyder, and S. Ryu, Rev. Mod. Phys. **88**, 035005 (2016).
[5] K. v. Klitzing, G. Dorda, and M. Pepper, Phys. Rev. Lett. **45**, 494 (1980).
[6] D. J. Thouless, M. Kohmoto, M. P. Nightingale, and M. den Nijs, Phys. Rev. Lett. **49**, 405 (1982).
[7] C. L. Kane and E. J. Mele, Phys. Rev. Lett. **95**, 146802 (2005).
[8] C. L. Kane and E. J. Mele, Phys. Rev. Lett. **95**, 226801 (2005).
[9] B. A. Bernevig and S.-C. Zhang, Phys. Rev. Lett. **96**, 106802 (2006).
[10] L. Fu, C. L. Kane, and E. J. Mele, Phys. Rev. Lett. **98**, 106803 (2007).
[11] M. König, S. Wiedmann, C. Brüne, A. Roth, H. Buhmann, L. W. Molenkamp, X.-L. Qi, and S.-C. Zhang, Science **318**, 766 (2007).
[12] H. Zhang, C.-X. Liu, X.-L. Qi, X. Dai, Z. Fang, and S.-C. Zhang, Nature Physics **5**, 438 (2009).
[13] L. Fu, Phys. Rev. Lett. **106**, 106802 (2011).
[14] T. H. Hsieh, H. Lin, J. Liu, W. Duan, A. Bansi, and L. Fu, Nature Communications **3**, 982 (2012).
[15] Y. Tanaka, Z. Ren, T. Sato, K. Nakayama, S. Souma, T. Takahashi, K. Segawa, and Y. Ando, Nature Physics **8**, 800 (2012).
[16] X. Wan, A. M. Turner, A. Vishwanath, and S. Y. Savrasov, Phys. Rev. B **83**, 205101 (2011).
[17] Z. Wang, Y. Sun, X.-Q. Chen, C. Franchini, G. Xu, H. Weng, X. Dai, and Z. Fang, Phys. Rev. B **85**, 195320 (2012).
[18] Z. Wang, H. Weng, Q. Wu, X. Dai, and Z. Fang, Phys. Rev. B **88**, 125427 (2013).
[19] S. M. Young, S. Zaheer, J. C. Y. Teo, C. L. Kane, E. J. Mele, and A. M. Rappe, Phys. Rev. Lett. **108**, 140405 (2012).
[20] J. A. Steinberg, S. M. Young, S. Zaheer, C. L. Kane, E. J. Mele, and A. M. Rappe, Phys. Rev. Lett. **112**, 036403 (2014).
[21] Z. K. Liu, B. Zhou, Y. Zhang, Z. J. Wang, H. M. Weng, D. Prabhakaran, S. K. Mo, Z. X. Shen, Z. Fang, X. Dai, Z. Hussain, and Y. L. Chen, Science **343**, 864 (2014).
[22] Z. K. Liu, J. Jiang, B. Zhou, Z. J. Wang, Y. Zhang, H. M. Weng, D. Prabhakaran, S. K. Mo, H. Peng, P. Dudin, T. Kim, M. Hoesch, Z. Fang, X. Dai, Z. X. Shen, D. L. Feng, Z. Hussain, and Y. L. Chen, Nature Materials **13**, 677 (2014).
[23] M. Neupane, S.-Y. Xu, R. Sankar, N. Alidoust, G. Bian, C. Liu, I. Belopolski, T.-R. Chang, H.-T. Jeng, H. Lin, A. Bansil, F. Chou, and M. Z. Hasan, Nature Communications **5** (2014).
[24] A. A. Soluyanov, D. Gresch, Z. Wang, Q. Wu, M. Troyer, X. Dai, and B. A. Bernevig, Nature **527**, 495 (2015).
[25] G. Kresse and J. Hafner, Phys. Rev. B **47**, 558 (1993).
[26] G. Kresse and J. Furthmüller, Phys. Rev. B **54**, 11169 (1996).
[27] P. E. Blöchl, Phys. Rev. B **50**, 17953 (1994).
[28] J. P. Perdew, K. Burke, and M. Ernzerhof, Phys. Rev. Lett. **77**, 3865 (1996).
[29] P. Durussel, R. Massara, and P. Feschotte, Journal of Alloys and Compounds **215**, 175 (1994).
[30] P. Blaha, K. Schwarz, P. Sorantin, and S. Trickey, Computer Physics Communications **59**, 399 (1990).

[31] J. P. Jan and A. Wenger, Phys. Rev. B **14**, 5182 (1976).
[32] A. Atrei, U. Bardi, G. Rovida, M. Torrini, E. Zanazzi, and P. N. Ross, Phys. Rev. B **46**, 1649 (1992).
[33] J. Kuntze, S. Speller, W. Heiland, A. Atrei, I. Spolveri, and U. Bardi, Phys. Rev. B **58**, R16005 (1998).
[34] W. C. A. N. Ceelen, A. W. Denier van der Gon, M. A. Reijme, H. H. Brongersma, I. Spolveri, A. Atrei, and U. Bardi, Surface Science **406**, 264 (1998).
[35] M. Hoheisel, J. Kuntze, S. Speller, A. Postnikov, W. Heiland, I. Spolveri, and U. Bardi, Phys. Rev. B **60**, 2033 (1999).
[36] M. Hoheisel, S. Speller, J. Kuntze, A. Atrei, U. Bardi, and W. Heiland, Phys. Rev. B **63**, 245403 (2001).
[37] M. Hoheisel, S. Speller, W. Heiland, A. Atrei, U. Bardi, and G. Rovida, Phys. Rev. B **66**, 165416 (2002).
[38] M. Hoheisel, S. Speller, A. Atrei, U. Bardi, and G. Rovida, Phys. Rev. B **71**, 035410 (2005).
[39] Y. Liu, D. Li, V. R. Stamenkovic, S. Soled, J. D. Henao, and S. Sun, ACS Catalysis **1**, 1719 (2011).
[40] H. L. Skriver, Phys. Rev. B **14**, 5187 (1976).
[41] B.-J. Yang and N. Nagaosa, Nature Communications **5**, 1 (2014).
[42] G. Bir and G. Pikus, *Symmetry and Strain-induced Effects in Semiconductors*, A Halsted Press book (Wiley, 1974).
[43] C.-C. Liu, H. Jiang, and Y. Yao, Phys. Rev. B **84**, 195430 (2011).
[44] J. Zhao, H. Liu, Z. Yu, R. Quhe, S. Zhou, Y. Wang, C. C. Liu, H. Zhong, N. Han, J. Lu, Y. Yao, and K. Wu, Progress in Materials Science **83**, 24 (2016).
[45] C.-C. Liu, W. Feng, and Y. Yao, Phys. Rev. Lett. **107**, 076802 (2011).
[46] L. Fu and C. L. Kane, Phys. Rev. B **76**, 045302 (2007).
[47] Y. Wu, L.-L. Wang, E. Mun, D. D. Johnson, D. Mou, L. Huang, Y. Lee, S. L. Bud'ko, P. C. Canfield, and A. Kaminski, Nature Physics **12**, 667 (2016).